15th World Congress on Computational Mechanics (WCCM-XV)
8th Asian Pacific Congress on Computational Mechanics (APCOM-VIII)
Virtual Congress: 31 July – 5 August 2022
S. Koshizuka (Ed.)

# PROPOSAL OF CRACK PROPAGATION CRITERION CONSIDERED CONSTRAINT EFFECT UNDER EXTREMELY LOW CYCLE FATIGUE; EVALUATION BY 1.5T-CT SPECIMEN

**K. KIDA[1], Y.WADA[2]**

[1] Kindai University
Higashi-Osaka, Osaka, Japan
kida.mech@kindai.ac.jp

[2] Kindai University
Higashi-Osaka, Osaka, Japan
wada@mech.kindai.ac.jp

**Key words:** Extremely low cycle fatigue, Fracture criterion, Constraint effect, Finite element analysis, Stress triaxiality, Equivalent plastic strain increment

**Abstract.** *The prediction of fracture behavior under extremely low cycle fatigue due to excessive loading is necessary for the life assessment of structures. This study evaluates the validity of the crack propagation criterion proposed in a previous study by performing generation phase and application phase analysis based on the results of fracture tests on a 1.5T-CT specimen (SGV410). The analysis show that the crack propagation criterion in the previous study predicted the experimental behavior well, however crack shape was incomplete in reproducing the crack shape.*

## 1 INTRODUCTION

The prediction of fracture behaviour under extremely low cycle fatigue due to excessive loading is necessary for the life assessment of structures. ΔJ criterion has been used to assess the life under low cycle fatigue. However, the applicability of this method is not well confirmed under extremely low cycle fatigue. Fracture toughness is dependent on the loading conditions and geometry due to the constraint effect.

The previous study (Ueda et al. [2]) focused on the physical quantities near the crack tip. These are the stress triaxiality $\sigma_{\mathrm{tri}}$ and the equivalent plastic strain increment $\Delta\varepsilon_{\mathrm{eq}}$. The former is a parameter related to the growth of voids in ductile fracture, while the latter is a parameter that indicates the degree of plastic deformation.

$$F_{\mathrm{elcf}} = {\Delta\varepsilon_{\mathrm{eq}}}^{m} + A\left({\delta}/{a_0}\right){\sigma_{\mathrm{tri}}}^{1-m} \geq B\left({a}/{a_0}\right) - C \tag{1}$$

where $\delta$ is load-line displacement, $a_0$ is initial crack length, and $a_0$ is crack length. $A$ and $m$ are the material constant values. $B$ and $C$ are parameters obtained by linear approximation of $F_{\mathrm{elcf}}$ and ${a}/{a_0}$.

Validity was confirmed under certain conditions. However, the crack shape could not be reproduced. Furthermore, different materials and specimen geometries have not been studied.

In this paper, the objective is to evaluate the validity of the crack propagation criterion (1) by applying it to CT specimens of different thicknesses and materials.

## 2 EXPERIMENT AND NUMERICAL ANALYSIS

### 2.1 Experiment

Fracture tests on CT specimens with a thickness of 1.5 inches (1.5T-CT specimens) conducted by the MDF Subcommittee [3] are subject to the simulation. Fig. 1 illustrates the geometry of the 1.5T-CT specimen. The material is SGV410, one of the typical steel grades used in nuclear equipment. The experimental conditions were load 60 kN, stress ratio $R = -1$, and the number of cycles leading to rupture $N_f$ was 22.

Fig. 2 and Fig. 3 shows the result of experiment. Evaluating simulation result uses them.

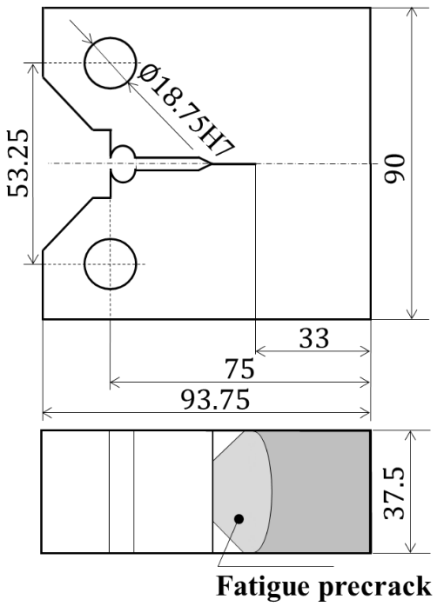


**Fig.1**:The geometry of 1.5T-CT specimen

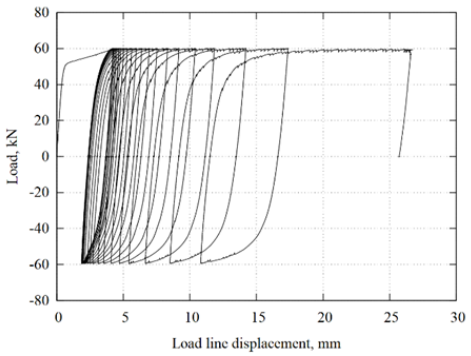


**Fig.2**: Load and load-line displacement of experiment


**Fig.3**: Fracture surface after experiment

### 2.2 Generation phase analysis

Fig. 4 shows the finite element model of the 1.5T-CT specimen created in this study. The numerical model is a quarter model that considers symmetry into account to reduce computational cost. Table.1 explains model details.

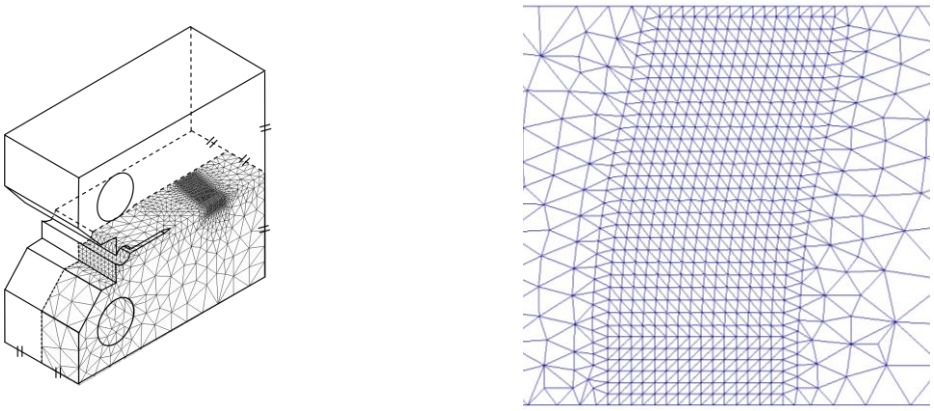

(a) Overall view of the finite element model (b) Crack front shape

**Fig.4**: Finite element model

**Table.1**:Finite element mode details

| Element type | Number of nodes | Number of elements | Minimum mesh size |
|---|---|---|---|
| Quadratic Tetrahedral Element | 30150 | 19975 | 0.6 mm |

In addition, the crack front shape is a curved shape (tunneling shape), which were determined by averaging the initial and final crack shapes based on the appearance of the fracture surface after the experiment. The reason for this is to obtain precise physical quantities.

The crack propagation simulation method is the nodal release method. The cracks propagate in a single line up to the next crack front position. The crack propagation condition is the relationship between the maximum load-line displacement and the amount of crack growth for each cycle.(Fig.5) These relationships changed the approximate curves in three parts. (Table.2) The first is the crack blunting process (I), the second is stable ductile fracture (III), and the third is unstable ductile fracture (V).

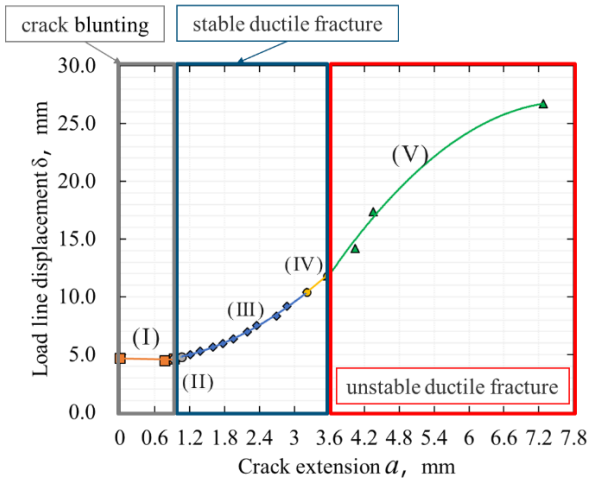


**Fig.5**: Crack propagation criterion in generation phase analysis

**Table.2**: Fitting function

| No. | Fitting function |
|---|---|
| I | $\delta = -0.08290a + 4.6588$ |
| II | $\delta = 1.179a + 3.552$ |
| III | $\delta = 0.6662a^2 - 0.2622a + 4.358$ |
| IV | $\delta = 4.174a - 3.018$ |
| V | $\delta = -0.8820a^2 + 13.63a - 25.74$ |

Table.3 shows material propaties of SGV410. The material hardening model is a combined hardening law that combines an isotropic hardening law and a nonlinear kinematics hardening law.

An isotropic hardening law are express as follows:

$$\sigma_i{}' = \left(\sigma_i - \sigma_{ys}\right) \times Q + \sigma_{ys} \quad (i \geq 2) \tag{2}$$

where $\sigma_{ys}$ is yield stress, $\sigma_i$ is true stress determined by n-th power hardening law from tensile test results (Fig. 5), $Q$ (=0.09) is contribution of isotropic hardening law.

The kinematics hardening law was the Chaboche law, which is the addition of the back stress components of the Armstrong-Frederick law.

$$\alpha = \sum_{i=1}^{n} \dot{\alpha_\iota} = \frac{2}{3}\sum_{i=1}^{n} (C_i \dot{\varepsilon}^{pl} - \gamma_i \dot{\bar{\varepsilon}}^{pl} \alpha_i) \tag{3}$$

where $C_i$ and $\gamma_i$ are material parameters (Table.4), $\dot{\varepsilon}^{pl}$is the plastic strain rate, and $\dot{\bar{\varepsilon}}^{pl}$ is the magnitude of the plastic strain rate.

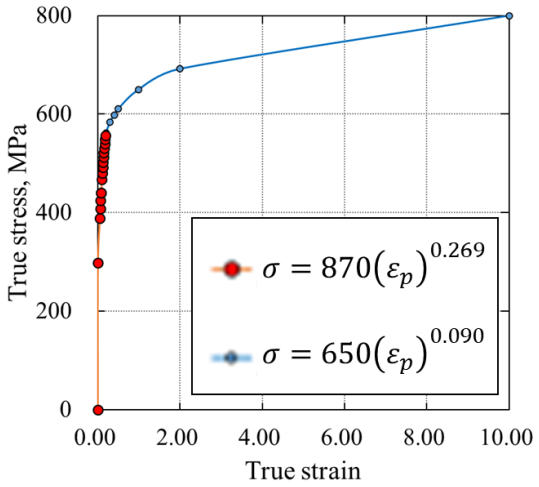


**Fig.6**: Relationships of true stress and strain determined by n-th power hardening law from tensile test results

**Table. 3**: Material properties of SGV410

| material properties | |
|---|---|
| Young modulus | 203 GPa |
| Poisson ratio | 0.3 |
| Yield stress | 298 MPa |

**Table. 4**: the parameters of the Chaboche law

| $i$ | $C_i$ | $\gamma_i$ |
|---|---|---|
| 1 | $2.34 \times 10^9$ | 9.10 |
| 2 | $4.34 \times 10^7$ | 1.63 |
| 3 | $1.22 \times 10^7$ | 0.325 |

A five-point moving average was computed at each crack location for the physical quantities obtained from three columns one element away from the crack tip. This calculation is performed by taking the average value between five adjacent points as the value of that point, in order to reduce the scatter of the data caused by the tetrahedral quadratic elements.

Next, an integral average is performed for the three points in the direction of crack propagation. The formula for integral average is given as

$$p_i = \frac{1}{\Delta a}\int_{a_{i+1}}^{a_{i+3}} p\mathrm{d}a \qquad (4)$$
$$\Delta a = a_{i+3} - a_{i+1}$$

where $p_i$ is the physical quantity of the i-th main node from the center of the thickness direction. (Fig.7) This reduces the specificity of the physical quantity near the crack tip and the element size dependence.

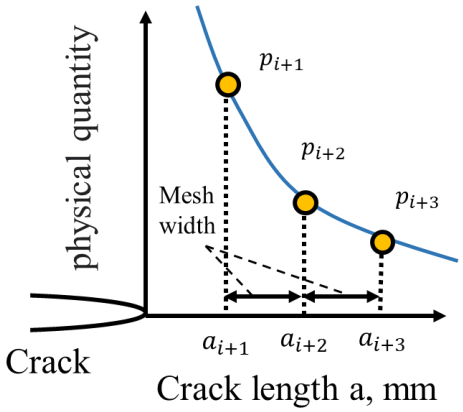


**Fig. 7**: Description of Integral average

## 2.3 Application phase analysis

The application phase analysis evaluates two different models of crack front shape. (Fig.8) Case.1 is the same model as in the Generation phase analysis, and case.2 is a model in which the crack front shape is straight.

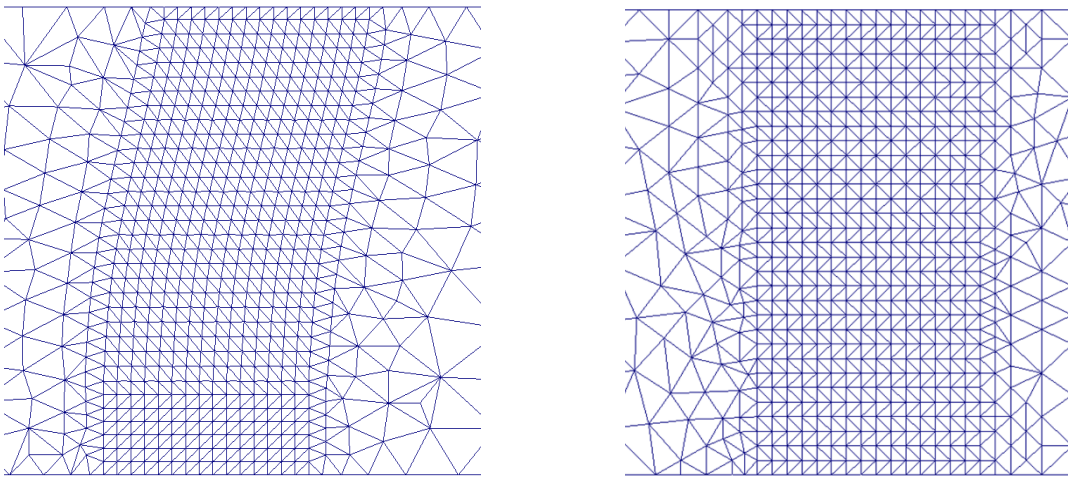

(a) case 1(tunneling shape) (b) case 2(straight line shape)

**Fig.8**: Crack length relationship for each cycle

In the application phase analysis, previous research evaluated only the nodal point one element away from the crack tip. In contrast, the evaluation nodes in this study are three rows of nodes in the direction of crack propagation, starting from the main node one element away from the crack tip. When the crack propagation criterion is satisfied, the nodal constraint perpendicular to the crack face is partially released and the crack propagates. Fig. 9 describes the method of crack propagation in the center of the thickness, on the surface side, and in other areas.

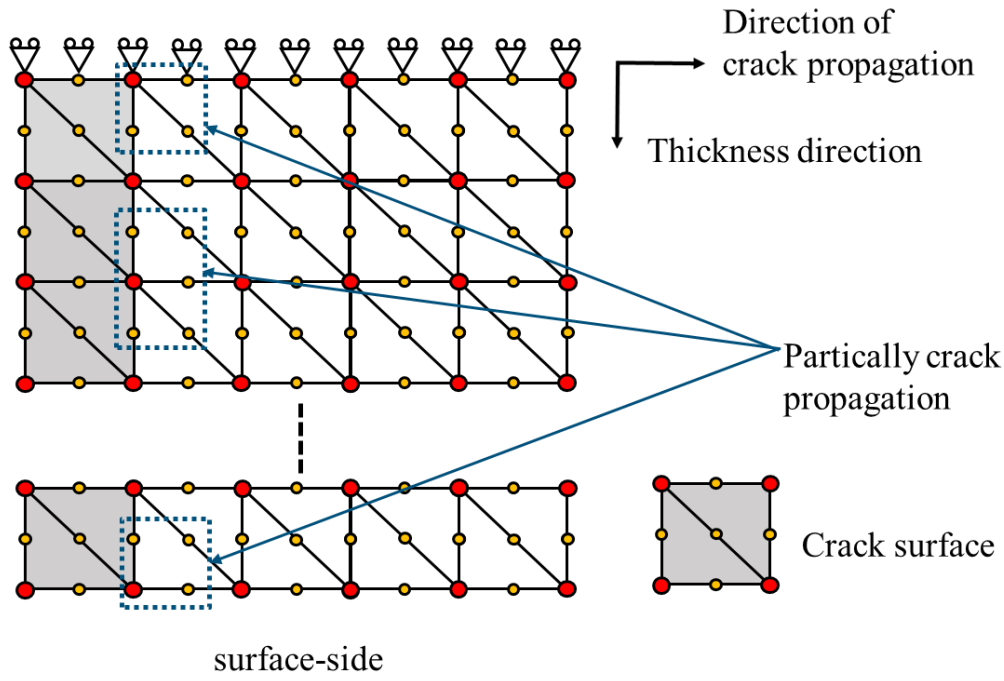


**Fig. 9**: Method of crack propagation in application phase analysis

Moreover, since the application phase analysis involves partial propagation of the crack, it is necessary to define the crack length. When the simulation step is step j, the crack length $a_j$is defined in the following.

$$a_j = a_{j-1} + \sum_{k}^{l} \alpha_k$$
$$\alpha_j = 2 \times \frac{L^2}{B} \tag{5}$$

where $l$ is the number of main nodes in thickness direction is mesh size, and B is thickness.

The crack propagation of 1 cycle is made in a row at the same release point as in the generation phase analysis. The reason for this is that the crack propagation behavior shown in Fig. 5 is different from that of stable ductile fracture in the initial stage.

## 3 RESULTS AND DISCUSSIONS

### 3.1 Results of generation phase analysis

Fig. 10 showed the comparison of experimental and numerical results of load and load-line displacement relationships. The initial cycle was overestimated. However, as the cycles increased and entered the stable ductile fracture, the tensile process was in good agreement.

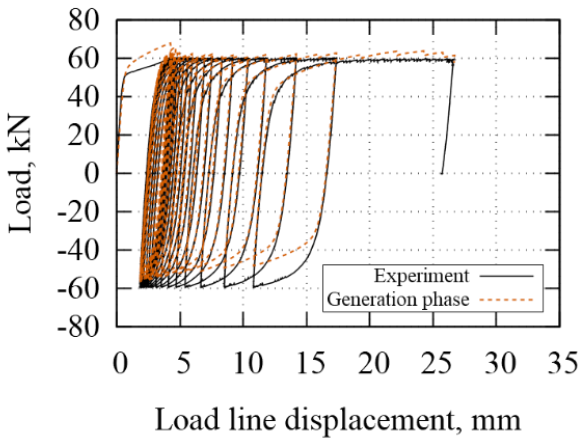


**Fig. 10**: Comparison of experimental and numerical results of load and load-line displacement relationships

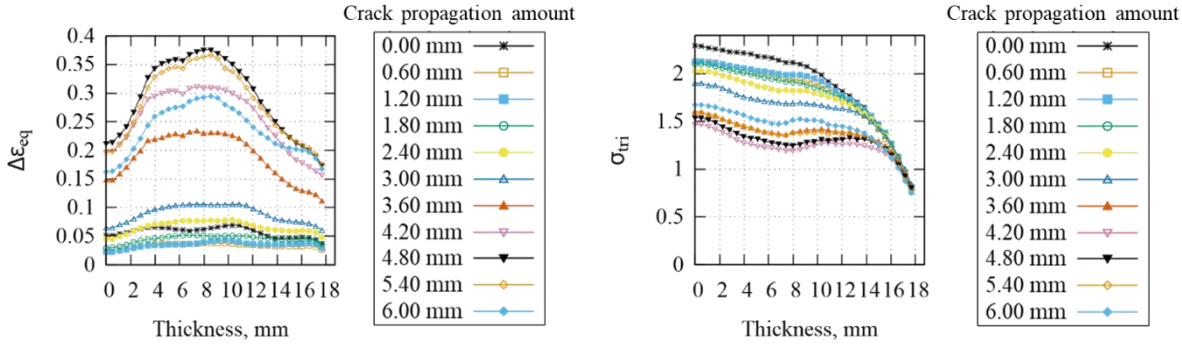


(a) (b)

**Fig. 11**: Thickness direction distribution of physical quantities at crack propagation (a) equivalent plastic strain, (b) stress triaxiality

Fig.11 illustrates thickness distribution of physical quantities at crack propagation. $\Delta\varepsilon_{\mathrm{eq}}$is large in the middle of the thickness direction and the middle of the surface side. By contrast, $\sigma_{\mathrm{tri}}$ reached a maximum in the center of the thickness direction, decreased as it approached the surface side, and reached a minimum on the surface side.

### 3.2 Determination of crack propagation criterion

Using the physical quantities obtained from the generation phase analysis determined the

parameters of the crack propagation criterion. (Fig.12) $A$,$m$ are the same as in the previous study. ($A = 0.55, m = 0.1$) The legend indicates the distance from the center of the thickness direction. Thereby $B$ and $C$ varied in the thickness direction, and these were determined by a linear approximation of the distribution in the thickness direction. (Fig.13)

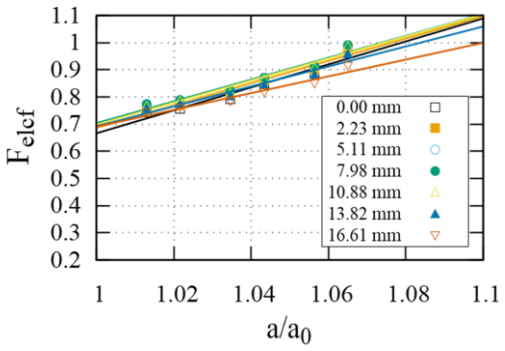


**Fig. 12**: Determination of crack propagation criterion

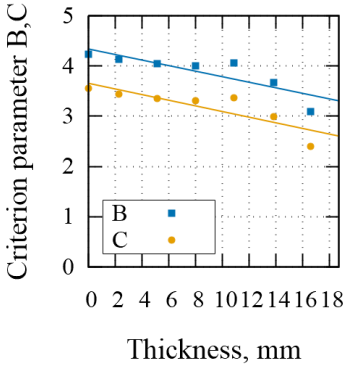


**Fig. 13**: Thickness direction distribution of $B$ and $C$

### 3.3 Results of application phase analysis and discussions

In the application phase analysis, the simulation stopped early because the final crack position was reached.

Fig.14 indicated that the crack lengths for each cycle were in good agreement for both Case.1 and Case.2. On the other hand, Fig.14 is that the crack propagation is faster than the experimental value as it approaches the final cycle.

On the contrary, Fig.15 showed that the crack propagates in the center of the thickness and on the surface side, not in the center of the thickness direction as shown in Fig.15. In addition, the crack propagation on the surface side stopped in the middle of the crack.

Therefore, the crack propagation criterion (1) is valid as an equation for predicting extremely low-cycle fatigue fracture, as shown in Fig.14. On the other hand, the reproducibility of the crack shape is incomplete and needs to be modified (Fig.15). Fig.13 indicates that the critical value of the crack propagation criterion depends on the thickness direction. This is explained by the dependence of the physical quantities in Fig.11 on thickness. For this reason, a parameter related to the constraint effect of thickness should be introduced.

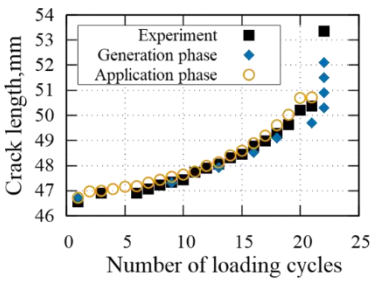


(a) case 1(tunneling shape)

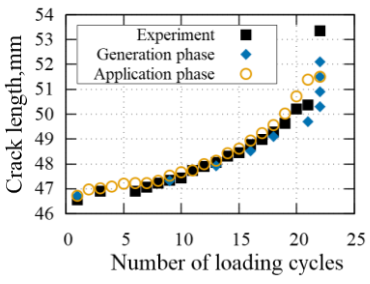


(b) case 2(straight line shape)

**Fig.14**: Crack length relationship for each cycle

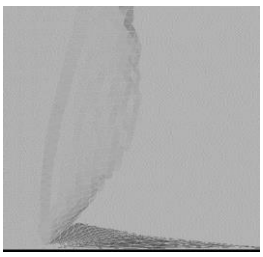

(a) case 1(tunneling shape)

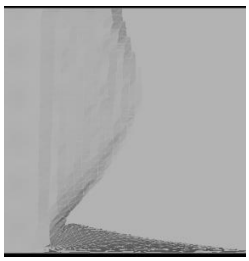

(b) case 2(straight line shape)

**Fig.15**: Crack shape at maximum load-line displacement for each cycle

## 4 CONCLUSIONS

In this research, the crack propagation criterion (1) were validated by generation phase and application phase anslysis of a 1.5T-CT specimen. The results showed good prediction of the crack growth behavior for each cycle, however, the reproducibility of the crack shape was incomplete. Therefore, the criterion needs to be improved by introducing new parameters to predict extremely low-cycle fatigue failure. For example, a parameter should be introduced to consider the constraint effect of thickness. In the future, since both the previous study and the present study were only conducted on CT specimens, the applicability to other specimens should be investigated.

## REFERENCES

[1] Dowling, N.E., and J.A. Begley. Fatigue Crack Growth During Gross Pasticity and the J-integral. ASTM STP (1976) 590, 82-103.

[2] Yoshitaka, W. and Kaito, U. Investigation of Fracture Criteria for Crack Propagation under Very Low Cycle Fatigue. *The 3rd International Conference on COMPSAFE* (2020)

[3] MDF Subcommittee. Research on Ductile Fracture under Multi-Axial State of Stress for Component and Structure of Light Water Reactor (2014)